

Numerical finite-difference time-domain calculation for extreme enhancement of magneto-optical effect at ultraviolet wavelength using Ni-subwavelength grating on SiO₂/Ni structure

Yuusuke Takashima^{1,2}, Masanobu Haraguchi^{1,2}, Yoshiki Naoi^{1,2}

¹Graduate School of Technology, Industrial and Social Science, Tokushima University, 2-1 Minami-josanjima, Tokushima 770-8506, Japan

²Institute of Post-LED Photonics, Tokushima University, 2-1 Minami-josanjima, Tokushima 770-8506, Japan

E-mail: takashima@tokushima-u.ac.jp

Abstract

An extreme enhancement of the polar Kerr magneto-optical (MO) effect was numerically demonstrated using surface plasmon polaritons (SPPs) at the SiO₂/Ni interface combined with the Ni-subwavelength grating (SWG). Utilizing the ω - k dispersion relation for the SPP at the SiO₂/Ni interface, the parameters of Ni-SWGs were designed to couple the SPP mode with the incident light. The electromagnetic field distribution was calculated using the finite-difference time-domain method to estimate and discuss the enhancement of MO effect in the designed structure. The results indicated that the reflectance of light for the designed structure dramatically decreased owing to SPP excitations. The field distributions revealed that the high electric field of the SPP was concentrated not only on the Ni substrate but also on Ni-SWG, yielding Kerr rotation angle 224 times higher than that without SPP. The results provide a new method for enhancing the MO effect; the extremely large MO enhancement achieved by our structure has a great potential for use in a wide range of applications.

Keywords: magneto-optical effect, subwavelength grating, surface plasmon polariton, polar Kerr effect.

1. Introduction

Magneto-optical (MO) effects, such as the polar Kerr effect, have been widely utilized in various fields of applications, such as, optical isolators [1], bio-sensing [2], imaging [3], and recording [4]. From the perspective of classical physics, the driving force of MO effects is the Lorentz force resulting from the magnetization of ferromagnetic materials [5]. In magnetized ferromagnetic materials, light-induced electronic polarization is affected by the Lorentz force. This generates a dipole orthogonal to that induced by light; a non-diagonal dielectric constant of the ferromagnetic materials appears. The non-diagonal components indicate the strength of the MO effects of the ferromagnetic material. However, the values of the non-diagonal components are extremely small when compared to those of the diagonal components, because the Lorentz force resulting from the magnetization–light interaction is much weaker than the electrical one. The small non-diagonal dielectric constant restricts the application of the MO effects to a very narrow range. Hence, it is necessary to enhance the MO effect.

Various resonance phenomena have been used to enhance the MO effect. Surface plasmon polaritons (SPPs), which couples oscillating free electrons and light at the metal/dielectric interface, are frequently utilized to assist light–magnetization interactions [6-20]. The excitation of SPPs provides a high localized field at the metal/dielectric interface because the light energy is confined to the metal surface. Several studies have demonstrated the enhancement of the MO effect using the localized high field of SPPs in multiple metallic layers [6-8], nanodisks [9-12], gratings [13-17], and nano-ring cavities [18-20]. Others have achieved MO enhancement using light trapping in magneto photonic crystals (PhCs) [21-24]. Photonic band engineering of PhCs confines the light around ferromagnetic materials, and PhCs achieve MO enhancement and high transparency simultaneously.

Recent studies have shown that subwavelength dielectric meta-structures with high refractive index contrast enhance the MO effect. [25, 26]. Owing to their strong light confinement by high refractive index contrast, meta-structures can enhance both electric and magnetic fields without intrinsic ohm loss [27-29]. Barsukova *et al.* experimentally demonstrated enhancement MO effect via magnetic dipole Mie-resonance in a Ni–Si meta-structure [26]. However, most of the MO enhancements mentioned before are indirect, because the ferromagnetic materials and resonance structures are different and separated. This restricts the magnitude of enhancement.

In this study, we numerically achieved a significant enhancement of the polar Kerr MO effect using a SiO₂/Ni interface combined with a Ni-subwavelength grating (SWG). The high electric field of the SPP at the SiO₂/Ni-substrate assisted the light-magnetization interaction. In particular, the MO effect was directly and significantly enhanced by high electric field of the SPP because the plasmonic and ferromagnetic structure are same (In other words, Ni plays both roles of plasmonic resonance and ferromagnetic materials). We also designed the parameters of Ni-SWGs to couple the irradiated light with the SPPs. To reveal the MO enhancement performance, the electromagnetic field distribution inside the designed structure was calculated using the finite-difference time-domain (FDTD) method.

2. Design of Ni-SWG/SiO₂/Ni substrate structure

Figure 1 depicts the proposed Ni-SWG-combined SiO₂/Ni-substrate structure. A thin SiO₂ film was deposited on a thick Ni substrate. Ni was chosen as the plasmonic material owing to its ferromagnetic characteristics and high plasma frequency [30, 31]. Ni-SWG was arranged on the SiO₂-film as shown in Fig. 1. The symbols Λ , t_{SWG} and w in Fig. 1 represent the SWG period, thickness, and width, respectively. The thickness of the SiO₂-film is denoted as t_{SiO_2} . k_{SPP} is the wavenumber for the SPP mode at the interface between SiO₂ and the Ni substrate. We assumed that the incident plane wave with wavelength λ entered the structure from the air. The electric field of the incident light was x-polarized (red arrow in Fig. 1).

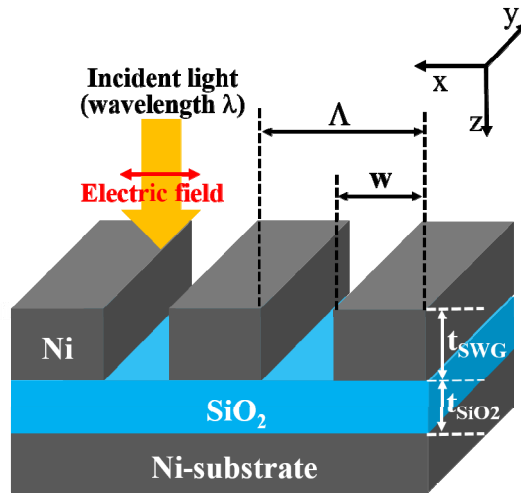


Fig.1 Schematic of the proposed Ni-SWG/SiO₂/Ni

The x-direction wave number of the diffractions resulting from the SWG is compensated by $2\pi m/\Lambda$, where m is the diffraction order. For SWG ($\Lambda < \lambda$), the higher-order ($|m| \geq 1$) diffractions become evanescent waves propagating along the $\pm x$ -direction [32]. Provided the wavenumbers of the higher diffractions coincide with that of SPP at the SiO₂/Ni-substrate, the diffractions couple with the SPP modes while the 0th-order diffraction is reflected by the SWG. On the other hand, the excited SPP is also re-radiated from the incident region by SWG, and the re-radiation interferes the 0th-order diffraction. The interference influences the reflectivity of the proposed structure. When the re-radiation and 0th reflected diffraction forms the destructive interference, the reflectivity at the SPP excitation wavelength dramatically decreases, because the energy of the light is confined at the interface between SiO₂ and the Ni substrate. The confinement of light energy also yields a high electric field at the interface.

When an external magnetic field is applied normally to our structure (along the z-direction), the Ni-SWG and Ni-substrate are magnetized. The magnetization leads to an electron oscillation orthogonal to that induced by the light; moreover, the non-diagonal components of the Ni dielectric constant appear.

The non-diagonal components are the origin of the MO effect and cause polarization rotation of the reflected light (which is called as “polar Kerr effect”). In particular, the high electric field of SPP at the SiO₂/Ni-substrate interface directly assists the interaction of light-magnetization, and it can significantly enhance the MO effect compared to the bulk material.

Based on the aforementioned enhancement principle, we selected the structural parameters of the Ni-SWG on the SiO₂/Ni-substrate such that the wavenumber of the 1st-order diffraction ($m = 1$) coincides with that of the SPP mode.

The the electromagnetic field continuity of the light gives the ω - k dispersion relation of SPP at the interface between SiO₂ and the Ni substrate, and is expressed as follows [33, 34]:

$$k_{SPP} = \left(\frac{\omega}{c}\right) \left(\frac{\epsilon_{Ni}\epsilon_{SiO_2}}{\epsilon_{Ni} + \epsilon_{SiO_2}}\right)^{1/2} \quad (1)$$

where ω and c represent the angular frequency of light and speed of light, respectively. The dielectric constants of SiO₂ and Ni are represented as ϵ_{SiO_2} and ϵ_{Ni} , respectively. The values of ϵ_{SiO_2} and ϵ_{Ni} were obtained from previous experimental results [30, 35].

Figure 2 shows the ω - k dispersion relation as a function of the incident wavelength. The black and red open circles in Fig. 2 mean the real and imaginary parts of the k_{SPP} , respectively.

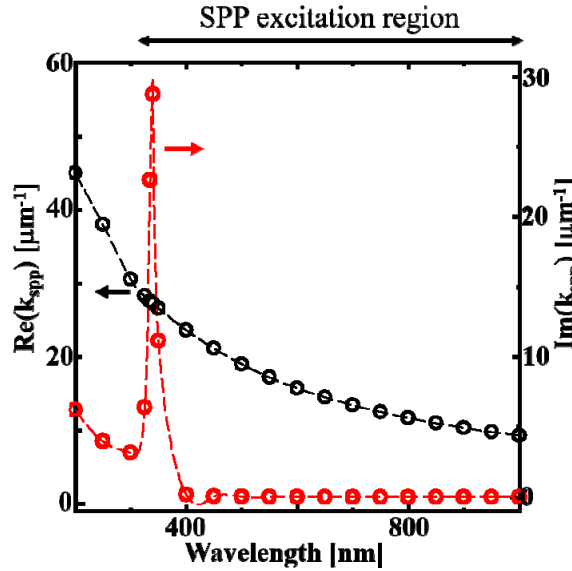


Fig.2 ω - k dispersion relation for the SPP mode at the SiO₂/Ni interface as a function of wavelength

The real part of k_{SPP} increases as the wavelength shortens, and the inflection point appears at a wavelength of approximately 325 nm. When the compensation of wavenumber by SWG matches the real

part of k_{SPP} , SPP can be excited. In addition, the imaginary part of k_{SPP} , namely propagation loss, rapidly increases at a wavelength of approximately 340 nm. The behavior of the real and imaginary parts indicates that the wavelength around 325 nm is the cutoff for the SPP, and one can excite the SPP at the longer wavelength region up to the cutoff wavelength. Figure 2 also shows that the properties of SPPs in visible and ultraviolet wavelength region are significantly different. For example, the SPP in ultraviolet region is near the cutoff wavelength, while that in visible range is not. To understand the role of the difference in the enhancement of MO effect more clearly we attempted to excite SPPs in the visible wavelength (645 nm) and ultraviolet (365 nm) wavelengths. To excite SPPs, the periods of the SWG were set to $\Lambda = 400$ nm and 200 nm for the excitation of the SPPs. Hence, a dip in reflectivity due to the excitation of SPPs is expected at each wavelength region. We also determined the thickness of SiO_2 and SWG as $t_{\text{SiO}_2} = 70$ nm and $t_{\text{SWG}} = 100$ nm, respectively, because very large values of t_{SiO_2} and t_{SWG} do not facilitate efficient coupling between the diffractions and the SPP.

To evaluate the enhancement of MO effect in our system, we performed finite-difference time-domain (FDTD) simulations of the electromagnetic field (*Poynting for Optics*: FUJITSU Co.).

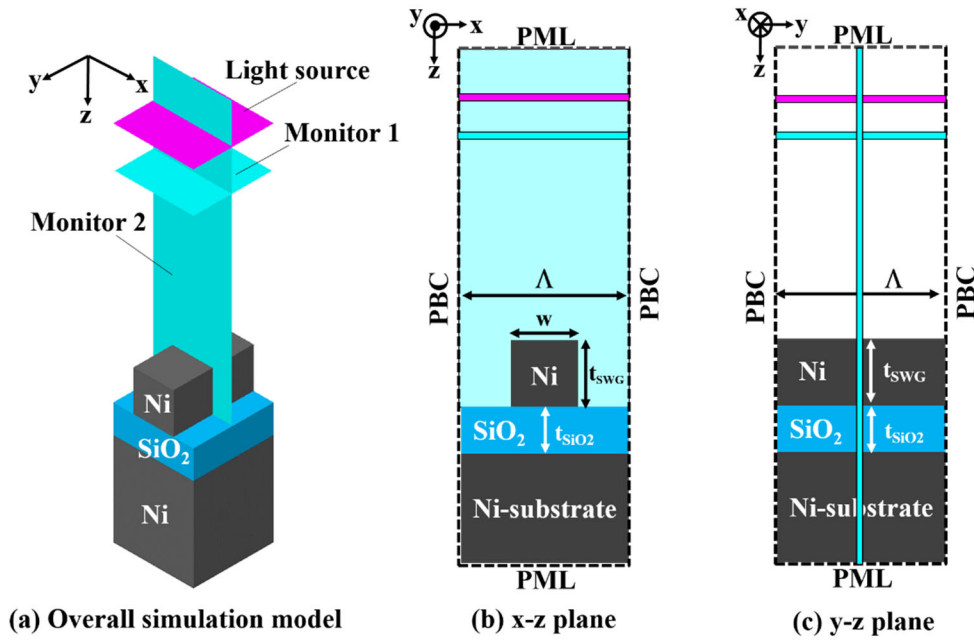


Fig.3 Schematic of FDTD simulation model.
(a) overall model (b) x-z plane (c) y-z plane.

Figure 3 shows the simulation model. We performed FDTD calculations of two models, such as model 1 and model 2, to investigate the MO enhancements by SPP modes in visible and ultraviolet wavelength regions. The structural parameters of the models are summarized in table 1. The filling factor FF is determined by w/Λ , and FF , t_{SWG} and t_{SiO_2} were fixed to 0.5, 100 nm and 70 nm, respectively. The designed Ni-SWG on the SiO_2/Ni -substrate was surrounded by the six boundaries represented by the

dashed lines in Fig. 3 (b) and (c). The perfectly matched layer (PML) boundary condition was applied in the $\pm z$ -direction.

The PMLs suppress the reflection of light at their surfaces because of impedance matching, and the incident light decreases rapidly. Thus, we can assume that the Ni substrate is infinitely thick. The periodic boundary condition (PBC), which infinitely repeats the fields, was set for the $\pm x$ - and $\pm y$ -directions. Therefore, our structure repeats infinitely in the $\pm x$ -direction, and the length of our structure is infinite in the $\pm y$ -direction. The incremental time grid Δt and space grids Δx , Δy , and Δz of FDTD simulation were set as $\Delta t = 7.38 \times 10^{-18}$ s and $\Delta x = \Delta y = \Delta z = 4$ nm.

Table 1 Parameters of the FDTD model

	Model 1 (for visible SPP)	Model 2 (for ultraviolet SPP)
Λ [nm]	400	200
w [nm]	200	100
t_{SWG} [nm]	100	100
t_{SiO_2} [nm]	70	70
FF (w/Λ)	0.5	0.5

We assumed the magnetization of Ni to be along the $+z$ -direction. Hence, the dielectric tensor of magnetized Ni is given by the following equation [31]:

$$\epsilon_{Ni} = \begin{pmatrix} \epsilon_{Ni, dia.} & \epsilon_{Ni, non-dia.} & 0 \\ -\epsilon_{Ni, non-dia.} & \epsilon_{Ni, dia.} & 0 \\ 0 & 0 & \epsilon_{Ni, dia.} \end{pmatrix} \quad (2)$$

where the symbols $\epsilon_{Ni, dia.}$ and $\epsilon_{Ni, non-dia.}$ are the diagonal and non-diagonal components of the Ni dielectric constant. In the FDTD calculation, the wavelength dispersion of diagonal component of ϵ_{Ni} was calculated by using well known Drude model and was given by following equation:

$$\epsilon_{Ni}(\omega) = 1 - \frac{\omega_p^2}{\omega^2 + i\Gamma\omega} \quad (3)$$

where ω_p represents plasma angular frequency of Ni. The symbol Γ is damping. We determined the value of ω_p and Γ by using the experimental refractive index and extinction coefficient of Ni at the reference wavelength [30]. The reference wavelength of 645 nm and 360 nm were used for determining the

wavelength dispersion of Ni in visible (model 1) and ultraviolet region (model 2), respectively (for example $\epsilon_{\text{Ni,dia}} = -2.57 + 8.11i$ at 360 nm, $-13.5 + 16.6i$ at 645 nm). The value of the non-diagonal components of ϵ_{Ni} were taken from previous studies ($\epsilon_{\text{Ni,non-dia}} = 0.040 + 0.048i$ at 360 nm and 645 nm) [31]. We also considered SiO₂ as nondispersive material with $\epsilon_{\text{SiO}_2} = 2.12 + 0i$ and $2.17 + 0i$ for model 1 (visible) and model 2 (ultraviolet) [35].

The x-polarized incident plane wave was normally irradiated onto the structure, and the reflected light intensity was calculated. The electric field of the reflected light is rotated by the non-diagonal dielectric tensor of the magnetized Ni (namely, polar Kerr MO effect). This rotation angle is the strength of the MO effect and is defined by

$$\theta = \tan^{-1}\left(\frac{E_y}{E_x}\right) \quad (4)$$

The E_x and E_y are the x- and y-component amplitudes of the electric field of the reflected light.

3. Results of Numerical Simulation and Discussions

Figure 4(a) and (b) show the calculated reflectivity and the Kerr rotation angle θ in the reflected light for the designed structures with $\Lambda = 400$ nm (model 1) and $\Lambda = 200$ nm (model 2), respectively. The black curves and blue circles correspond to the reflectivity and Kerr rotation angle, respectively. The insets of the Fig. 4(a) is definition of the Kerr rotation angle θ .

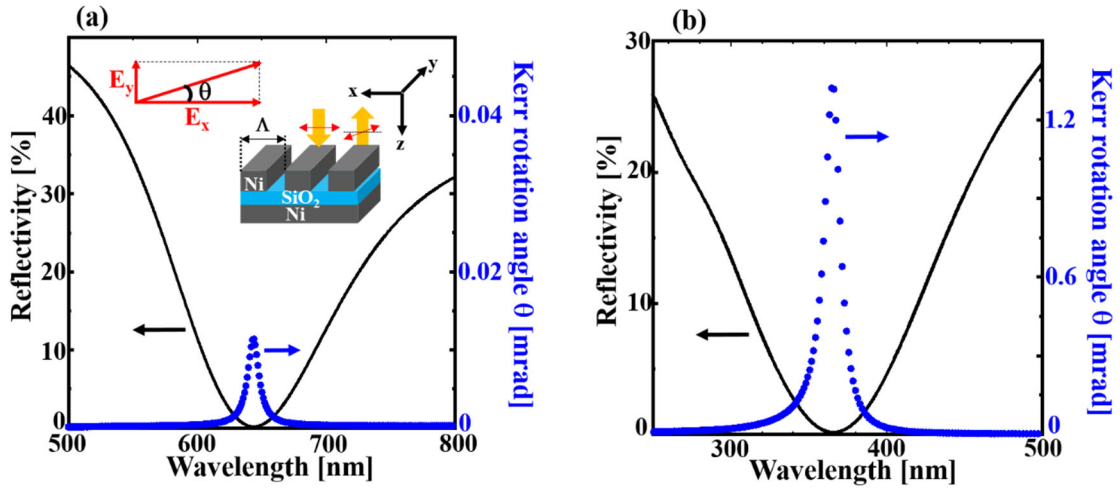


Fig.4 Reflectivity and Kerr rotation angle in our designed structure (a) with $\Lambda = 400$ nm, (b) $\Lambda = 200$ nm. The Kerr rotation angle is determined by the E_y to E_x amplitude in the reflected light at the structure

As shown in Fig 4(a) and (b), the reflectivity dramatically decreased at wavelengths of 645 nm and 365 nm. The dip in reflectivity at these wavelengths is in good agreement with the predictions from

the ω - k dispersion relation of SPP described in Section 2; these results provide evidence for the excitations of SPP at the SiO₂/Ni-substrate interface at each wavelength. Moreover, the sharp peaks of the Kerr rotation angle appear at the SPP excitation wavelength; the MO effect is enhanced compared to those at other wavelengths. In particular, the Kerr rotation angle at a wavelength of 365 nm is 224 times larger than that achieved with only Ni-substrate, whereas that at 645 nm wavelength is 32 times larger. This extremely high enhancement of the MO effect opens up the possibility of developing a new class of MO devices in the ultraviolet wavelength region, such as high-density memory.

Let us try to understand the reason behind the large enhancement of the MO effect. Figure 5(a) and (b) show the normalized z -component of the electric field distribution at each SPP wavelength because the field of the SPP strongly influences for the Kerr rotation in the reflected light. The z -components of the electric field are not present outside the designed structures because the propagation direction of the incident light is in the z -direction. In fact, z -component fields appear around the SWG and Ni-substrate surfaces. The z -component field distributions indicate that the SPP modes propagating along the x -direction exist at the SWG and the surface of Ni substrate.

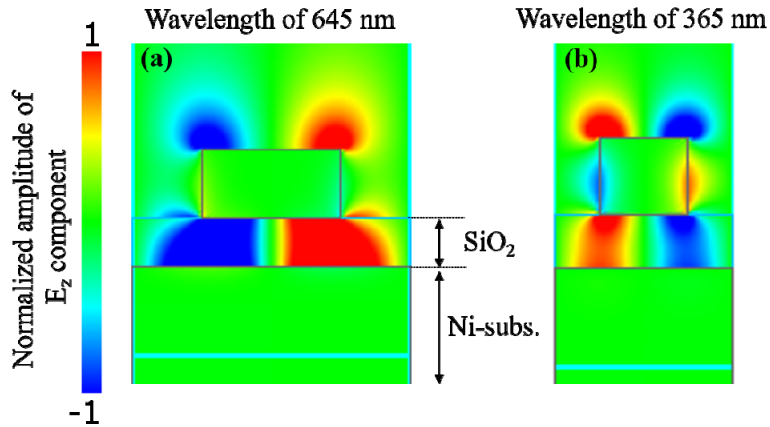


Fig.5 Normalized amplitude electric field of E_z components
(a) at 645 nm of wavelength (b) at 365 nm of wavelength

Thus, the distributions indicate the coupling between the diffracted light and the SPP mode propagating in the x -direction at the SiO₂/Ni-substrate. The excitation of SPP also causes energy confinement of the incident light around the SiO₂/Ni interface. At a wavelength of 645 nm, the SPP field was highly concentrated in the SiO₂ layer (see Fig. 5 (a)); whereas the SPP field at 365 nm is highly concentrated not only at the surface of the Ni substrate but also at Ni-SWG (Fig. 5 (b)). The field also appears at the Ni-SWG sidewalls, whereas the field of the visible wavelength SPP does not. This indicates that the excited ultraviolet SPP modes enhance the MO effect in both the Ni substrate and Ni-SWG. As a result, an extremely large enhancement of the MO response was achieved at a wavelength of 365 nm. The results suggest that the concentration of a high field in a ferromagnetic material plays a key role in the

enhancement of the light–magnetization interaction and provides a new method for the design of MO applications. Moreover, the figure of merit (FOM), which is defined as product of the Kerr rotation angle and square root of the reflectivity, is also important for actual applications. In further work, we will try to improve FOM while maintaining the enhancement of MO effect.

4. Conclusion

In conclusion, we numerically investigated the enhancement of the MO effect in Ni-SWG on a SiO₂/Ni-substrate. To excite the SPP mode at ultraviolet and visible wavelengths, the structural parameters of the SWG and SiO₂ thickness were designed via the ω -k dispersion relation for the SPP mode at the SiO₂/Ni-substrate. The FDTD calculated field distributions indicated the decreasing reflectivity of the designed structure associated with SPP excitation. The simulation also revealed that the electric field of SPP at a wavelength of 365 nm was highly concentrated on both the Ni substrate and Ni-SWG, yielding a 224-fold enhancement of the MO response compared to that without the SPP. These results provide a new method for MO enhancement; the significantly large MO enhancement of our structure has a great potential for use in a wide range of applications.

Acknowledgement

This work was partially supported by JSPS KAKENHI (Grant Number JP18K04238, JP21K14515).

Competing interesting

The authors declare no competing interests

References

1. Stadler, B.J.H., Mizumoto, T.: Integrated magneto-optical materials and isolators: a review. *IEEE Photonics J.* 6(1), 1–15 (2014)
2. Manera, M.G., Colombelli, A., Taurino, A., Martin, A.G., Rella, R.: Magneto-optical properties of noble-metal nanostructures: functional nanomaterials for bio sensing. *Sci. Rep.* 8(1), 12640 (2018)
3. Goa, P.E., Hauglin, H., Olsen, Å.A.F., Baziljevich, M., Johansen, T.H.: Magneto-optical imaging setup for single vortex observation. *Rev. Sci. Instrum.* 74(1), 141–146 (2003)
4. Jenkins, D., Clegg, W., Windmill, J., Edmund, S., Davey, P., Newman, D., Wright, C.D., Loze, M., Armand, M., Atkinson, R., Hendren, B., Nutter, P.: Advanced optical and magneto-optical recording techniques: a review. *Microsyst. Technol.* 10(1), 66–

75 (2003)

5. Pitaevskii, L.P., Lifshitz, E.M., Sykes, J.B.: Course of theoretical physics: physical kinetics. Elsevier
6. Bertrand, P., Hermann, C., Lampel, G., Peretti, J., Safarov, V.I.: General analytical treatment of optics in layered structures: application to magneto-optics. *Phys. Rev. B* 64(23) (2001). [235422](#)
7. González-Díaz, J.B., García-Martín, A., Armelles, G., García-Martín, J.M., Clavero, C., Cebollada, A., Lukaszew, R.A., Skuza, J.R., Kumah, D.P., Clarke, R.: Surface-magnetoplasmon nonreciprocity effects in noble-metal/ferromagnetic heterostructures. *Phys. Rev. B* 76(15) (2007). [153402](#)
8. Temnov, V.V., Armelles, G., Woggon, U., Guzatov, D., Cebollada, A., Garcia-Martin, A., Garcia-Martin, J.-M., Thomay, T., Leitenstorfer, A., Bratschitsch, R.: Active magneto-plasmonics in hybrid metal-ferromagnet structures. *Nature. Photon.* 4(2), 107–111 (2010)
9. Armelles, G., Cebollada, A., García-Martín, A., García-Martín, J.M., González, M.U., González-Díaz, J.B., Ferreiro-Vila, E., Torrado, J.F.: Magnetoplasmonic nanostructures: systems supporting both plasmonic and magnetic properties. *J. Opt. A: Pure Appl. Opt.* 11(11) (2009). [114023](#)
10. Rubio-Roy, M., Vlasin, O., Pascu, O., Caicedo, J.M., Schmidt, M., Goñi, A.R., Tognalli, N.G., Fainstein, A., Roig, A., Herranz, G.: Magneto-optical enhancement by plasmon excitations in nanoparticle/metal structures. *Langmuir* 28(24), 9010–9020 (2012)
11. Pourjamal, S., Kataja, M., Maccaferri, N., Vavassori, P., van Dijken, S.: Tunable magnetoplasmonics in lattices of Ni/SiO₂/Au dimers. *Sci. Rep.* 9(1), 9907 (2019)
12. Freire-Fernández, F., Kataja, M., Van Dijken, S.: Surface-plasmon-polariton-driven narrow-linewidth magneto-optics in Ni nanodisk arrays. *Nanophotonics* 9(1), 113–121 (2020)
13. Grunin, A.A., Zhdanov, A.G., Ezhov, A.A., Ganshina, E.A., Fedyanin, A.A.: Surface-plasmon-induced enhancement of magneto-optical Kerr effect in all-nickel subwavelength nanogratings. *Appl. Phys. Lett.* 97(26) (2010). [261908](#)
14. Belotelov, V.I., Akimov, I.A., Pohl, M., Kotov, V.A., Kasture, S.F., Vengurlekar, A.S., Gopal, A.V., Yakovlev, D.R., Zvezdin, A.K., Bayer, M.: Enhanced magneto-optical effects in magnetoplasmonic crystals. *Nat. Nanotechnol.* 6(6), 370–376 (2011)
15. Lei, C., Man, Z., Tang, S.: Extraordinary optical transmission and enhanced magneto-optical Faraday effects in one-dimensional metallic gratings. *Appl. Phys. Express* 13(12) (2020)

16. Frolov, A.Y., Shcherbakov, M.R., Fedyanin, A.A.: Dark mode enhancing magneto-optical Kerr effect in multilayer magnetoplasmonic crystals. *Phys. Rev. B* 101(4) (2020). [045409](#)
17. Takashima, Y., Moriiwa, K., Haraguchi, M., Naoi, Y.: Optical detection for magnetic field using Ni-subwavelength grating on SiO₂/thin-film Ag/glass structure. *Sci. Rep.* 10(1), 19298 (2020)
18. Feng, H.Y., Luo, F., Kekesi, R., Granados, D., Meneses-Rodríguez, D., García, J.M., García-Martín, A., Armelles, G., Cebollada, A.: Magnetoplasmonic nanorings as novel architectures with tunable magneto-optical activity in wide wavelength ranges. *Advanced. Optical. Materials.* 2(7), 612–617 (2014)
19. Feng, H.Y., Luo, F., Arenal, R., Henrard, L., García, F., Armelles, G., Cebollada, A.: Active magnetoplasmonic split-ring/ring nanoantennas. *Nanoscale* 9(1), 37–44 (2017)
20. López-Ortega, A., Zapata-Herrera, M., Maccaferri, N., Pancaldi, M., Garcia, M., Chuvilin, A., Vavassori, P.: Enhanced magnetic modulation of light polarization exploiting hybridization with multipolar dark plasmons in magnetoplasmonic nanocavities. *Light Sci. Appl.* 9(11), 49 (2020)
21. Fedyanin, A.A., Aktsipetrov, O.A., Kobayashi, D., Nishimura, K., Uchida, H., Inoue, M.: Enhanced Faraday and nonlinear magneto-optical Kerr effects in magnetophotonic crystals. *J. Magn. Magn. Mater.* 282(1–3), 256–259 (2004)
22. Levy, M., Li, R.: Polarization rotation enhancement and scattering mechanisms in waveguide magnetophotonic crystals. *Appl. Phys. Lett.* 89(12) (2006). [121113](#)
23. Goto, T., Baryshev, A.V., Inoue, M., Dorofeenko, A.V., Merzlikin, A.M., Vinogradov, A.P., Lisyansky, A.A., Granovsky, A.B.: Tailoring surfaces of one-dimensional magnetophotonic crystals: optical Tamm state and Faraday rotation. *Phys. Rev. B* 79(12) (2009). [125103](#)
24. Khokhlov, N.E., Prokopov, A.R., Shaposhnikov, A.N., Berzhansky, V.N., Kozhaev, M.A., Andreev, S.N., Ravishankar, A.P., Achanta, V.G., Bykov, D.A., Zvezdin, A.K., Belotelov, V.I.: Photonic crystals with plasmonic patterns: novel type of the heterostructures for enhanced magneto-optical activity. *J. Phys. D: Appl. Phys.* 48(9) (2015). [095001](#)
25. Barsukova, M.G., Shorokhov, A.S., Musorin, A.I., Neshev, D.N., Kivshar, Y.S., Fedyanin, A.A.: Magneto-optical response enhanced by Mie resonances in nanoantennas. *ACS Photonics* 4(10), 2390–2395 (2017)
26. Barsukova, M.G., Musorin, A.I., Shorokhov, A.S., Fedyanin, A.A.: Enhanced magneto-optical effects in hybrid Ni-Si metasurfaces. *APL Photonics* 4(1), 016102

- (2019)
27. Zhao, Q., Zhou, J., Zhang, F., Lippens, D.: Mie resonance-based dielectric metamaterials. *Mater. Today* 12(12), 60–69 (2009)
 28. Jahani, S., Jacob, Z.: All-dielectric metamaterials. *Nat. Nanotechnol.* 11(1), 23–36 (2016)
 29. Liu, T., Xu, R., Yu, P., Wang, Z., Takahara, J.: Multipole and multimode engineering in Mie resonance-based metastructures. *Nanophotonics* 9(5), 1115–1137 (2020)
 30. Johnson, P.B., Christy, R.W.: Optical constants of transition metals: Ti, V, Cr, Mn, Fe, Co, Ni, and Pd. *Phys. Rev. B* 9(12), 5056–5070 (1974)
 31. Krinchik, G.S., Artem'ev, V.A.: Magneto-optical properties of Ni, Co, and Fe in the ultraviolet visible, and infrared parts of the spectrum. *Sov. Phys. JETP* 26(6), 1080–1085 (1968)
 32. Kikuta, H., Toyota, H., Yu, W.: Optical elements with subwavelength structured surfaces. *Opt. Rev.* 10(2), 63–73 (2003)
 33. Sambles, J.R., Bradbery, G.W., Yang, F.Z.: Optical excitation of surface plasmons: an introduction. *Contemp. Phys.* 32(3), 173–183 (1991)
 34. Barnes, W.L., Dereux, A., Ebbesen, T.W.: Surface plasmon subwavelength optics. *Nature* 424(6950), 824–830 (2003)
 35. Malitson, I.H.: Interspecimen comparison of the refractive index of fused silica*. *J. Opt. Soc. Am.* 55(10), 1205–1208 (1965)